Reverse transcription–polymerase chain reaction

ISOGEN (Nippon Gene, Tokyo, Japan) was used to isolate total RNA and cDNA was synthesized with 5 μg of RNA in 20 μl of reaction buffer. The following primers were used for polymerase chain reaction (PCR) assay. SOD1, 5′-GACTGAAGGCCTGCATGGATTCC-3′ (forward) and 5′-CACAAGCCAAACGACTTCCAGCG-3′ (reverse); SOD2, 5′-GAGATGTTA CAGCCCAGATAG-3′ (forward) and 5′-AATCCCCAGCAGTGGAATAAGG-3′ (reverse); and $p21^{WAF1/CIP1}$, 5′-GACACCACTGGAGGGTGACT-3′ (forward) and 5′-CAGGTCCACATGGTCTTCCT-3′ (reverse). Human β-actin primers were 5′-GACTTAGTTGCGTTACACCC-3′ (forward) and 5′-CCTCCCCTGTGTGGACTTGG-3′ (reverse). Conditions for PCR were 94°C 1 min, 50°C 30 s, and 68°C 1 min, for 35 cycles.

Western blotting

Cells were lysed in 50 mmol/l Tris-HCl (pH 7.4), 1% SDS, 10 mmol/l EDTA, 1 mmol/l Na_3VO_4, 1 mmol/l NaF, 1 mmol/l phenylmethylsulfonyl fluoride, and 10 μg/ml aprotinin. Protein samples were resolved by SDS–polyacrylamide gel electrophoresis and transferred to membranes. They were stained with Ponceau S to detect transferred proteins, blocked, and probed with following antibodies: anti-poly (ADP-ribose) polymerase-1 (PARP-1) (Merck Biosciences), anti-microtubule-associated protein light chain 3 (MAP-LC3) (Medical & Biological Laboratories, Nagoya, Japan), anti-p53, anti-$p21^{WAF1/CIP1}$ (Merck Biosciences), and anti-phospho p53 (Ser15) (Cell Signaling Technologies, Danvers, MA). Blots were then incubated with peroxidase-labeled secondary antibody, and enzyme activity was detected by enhanced chemiluminescence (ECL) system (GE Healthcare UK, Buckinghamshire, UK).

Detection of ROS in NP-2 cells using dichlorofluorescein diacetate

NP-2 cells were washed with PBS, incubated at 37°C for 30 min with 10 μmol/l of dichlorofluorescein diacetate (DCFDA) (Invitrogen, Carlsbad, CA) in Hank's balanced salt solution (HBSS), and washed with PBS. Cells were then lysed with 0.1 mol/l KH_2PO_4/0.5% Triton X-100, and centrifuged at 12,000 rpm for 5 min. The supernatants were transferred to microplates and the fluorescence was measured using a spectrophotometer. To investigate the effect of α-tocopherol (α-Toc) (Sigma) on ROS formation, cells were trypsinized immediately after irradiation at 6 Gy, plated at 2×10^4 cells/well into 24-well tissue culture plates, cultured for 20 h, and treated with α-Toc for 24 h. The generation of ROS was determined as described above.

Staining of lysosomse

NP-2 cells were incubated with 100 nmol/l LysoTracker (Invitrogen) in HBSS for 30 min at 37°C, washed, and observed under a fluorescence microscope (CKX41; Olympus, Tokyo, Japan).

Staining of intracellular ROS with DCFDA

NP-2 cells were labeled with 10 μmol/l DCFDA, 100 nmol/l LysoTracker, and 1 μg/ml Hoechst 33342 in HBSS, washed, and, analyzed on slides under an All-in-One Type Fluorescence Microscope (BZ-8000; Keyence, Osaka, Japan) using the haze reduction function of BZ Analyzer Software (Keyence).

RESULTS

Effect of C-ion irradiation on the growth and morphological changes in NP-2 cells

Irradiation of NP-2 cells with C-ions showed a dose-dependent inhibition of growth of cells (Fig. 1A). The susceptibility of NP-2 cells to C-ion irradiation was examined by a clonogenic assay (Fig. 1B), and the D_{10} (10% survival dose) from the survival curve was determined to be 1.2 Gy.

We next examined the effect of C-ions irradiation on the morphological changes of NP-2 cells (Fig. 1C). As compared with nonirradiated cells or those irradiated at 1 Gy, morphological changes, including enlarged and flattened cell shape with abundant cytoplasm, were markedly apparent in cells irradiated at 6 Gy. The diameter of nonirradiated NP-2 cells was generally 5 to 8 μm, whereas those of giant cells formed after irradiation was 20 to 50 μm. Moreover, the giant cells consisted of either cells with a single large nucleus (single-nucleated giant cells [SNGCs]) or more than two nuclei (multinucleated giant cells [MNGCs]).

Induction of apoptosis and autophagy in NP-2 cells after irradiation with C-ions

To examine induction of apoptosis in NP-2 cells after irradiation with C-ions, we stained the nuclei with Hoechst 33342. As shown in Fig. 2A, nuclei with condensed chromatin as an apoptotic marker were clearly detected in NP-2 cells 5 days after irradiation at 6 Gy. It should be noted that chromatin condensation was not detected in SNGCs or MNGCs but that round-shaped cells that had been detached from dishes were identified as apoptotic cells. To confirm that the detached cells are apoptotic, we performed Western blotting to detect a cleaved PARP-1 fragment, a marker for apoptosis (Fig. 2B). Cell lysates prepared from detached cells showed a cleaved PARP-1 fragment (24 kDa) (Fig. 2B, lane 2), whereas lysates from attached cells did not (Fig. 2B, lane 1), indicating that apoptotic markers were detected in the detached cells. To quantify the incidence of apoptosis, cells with condensed chromatin were counted, and ratios of apoptotic cells were expressed as percentages of total cell counts. Apoptosis was induced in 10% of NP-2 cells 2 days after irradiation, and the incidence of apoptosis gradually increased in a time-dependent manner (Fig. 2C).

In addition to apoptotic cell death (programmed cell death Type I), autophagic cell death has been reported to be recognized as programmed cell death Type II (17). We next examined whether C-ions irradiation would induce autophagy in NP-2 cells. As a positive control for induction of autophagy, NP-2 cells were incubated in HBSS at 37°C for 2 h for amino acid starvation, a widely known procedure for induction of autophagy. After this treatment, the cells were labeled with monodansylcadaverine (MDC), a specific marker for autophagy (10,11). As shown in Fig. 2E, autophagic vacuoles were specifically detected as many MDC-positive, punctuated structures in the starved cells but not in the control cells (Fig. 2D). As shown in Fig. 2F, autophagic vacuoles were also detected in irradiated NP-2 cells (3 days after irradiation

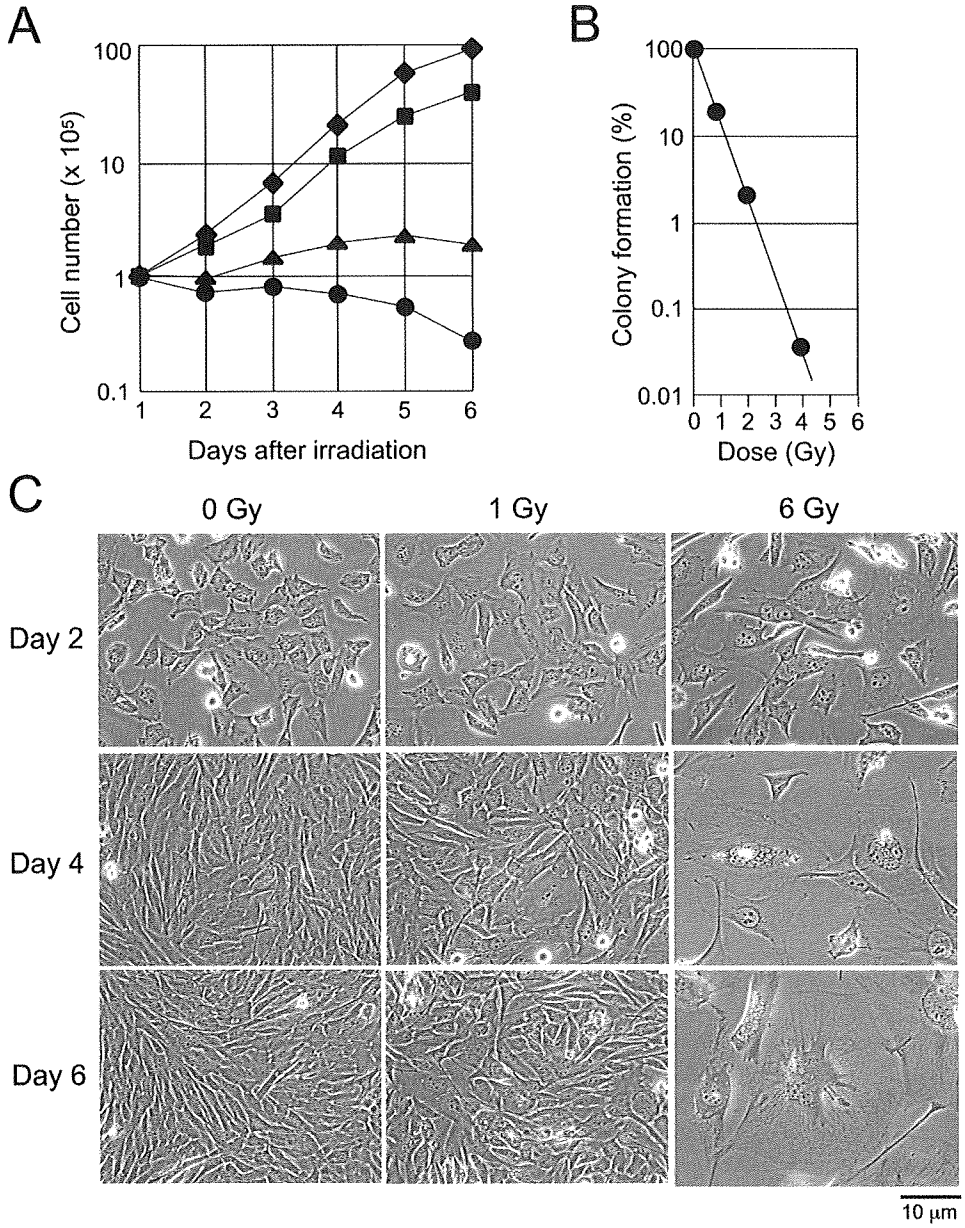

Fig. 1. Effect of C-ion irradiation on the growth and morphological changes of NP-2 cells. (A) NP-2 cells were irradiated with C-ions at 0 (◆) 1 (■), 3 (▲), or 6 (●) Gy, washed with phosphate-buffered saline and trypsinized, and the number of cells was counted on the days indicated. (B) Survival curve of NP-2 cells. The numbers of colonies were counted 10 days after irradiation. Experiments were done three times, and a representative result is shown. (C) Morphological changes in NP-2 cells after irradiation with C-ions. Irradiated cells were cultured and photographed on the days indicated.

at 6 Gy). Treatment of the irradiated cells with 3-methyladenine (3-MA), a specific inhibitor of early stages of the autophagic process (12), prevented the development of MDC-positive, dot-like structures (Fig. 2 G). The cells with MDC-positive autophagic vacuoles were detected in 20% of NP-2 cells 2 days after irradiation and dramatically increased 3 days after irradiation (Fig. 2 H). It is known that a critical event in autophagy is the conversion of microtubule-associated protein light chain 3 (MAP-LC3) (LC3-I, 18 kDa) to the membrane-bound form (LC3-II, 16 kDa) (13). As compared with nonirradiated cells (Fig. 2I, lane 1), increase in expression of LC3-I and accumulation of LC3-II form were detected in NP-2 cells 3 days after irradiation at 6 Gy (lane 2), indicating further the induction of autophagy in the irradiated NP-2 cells. Thus, these results indicated that C-ion irradiation induced not only apoptosis but also autophagy in NP-2 cells.

Specific expression of SA-β-gal in the enlarged NP-2 cells after C-ion irradiation

As mentioned above, when NP-2 cells were irradiated at 6 Gy, most cells died of apoptosis and autophagy (Fig. 2). The residual cells with enlarged and flattened appearance still attached to dishes (Fig. 1C), but they did not grow and could not form colonies, indicating that no surviving cells were detected. Because the morphological features of these enlarged

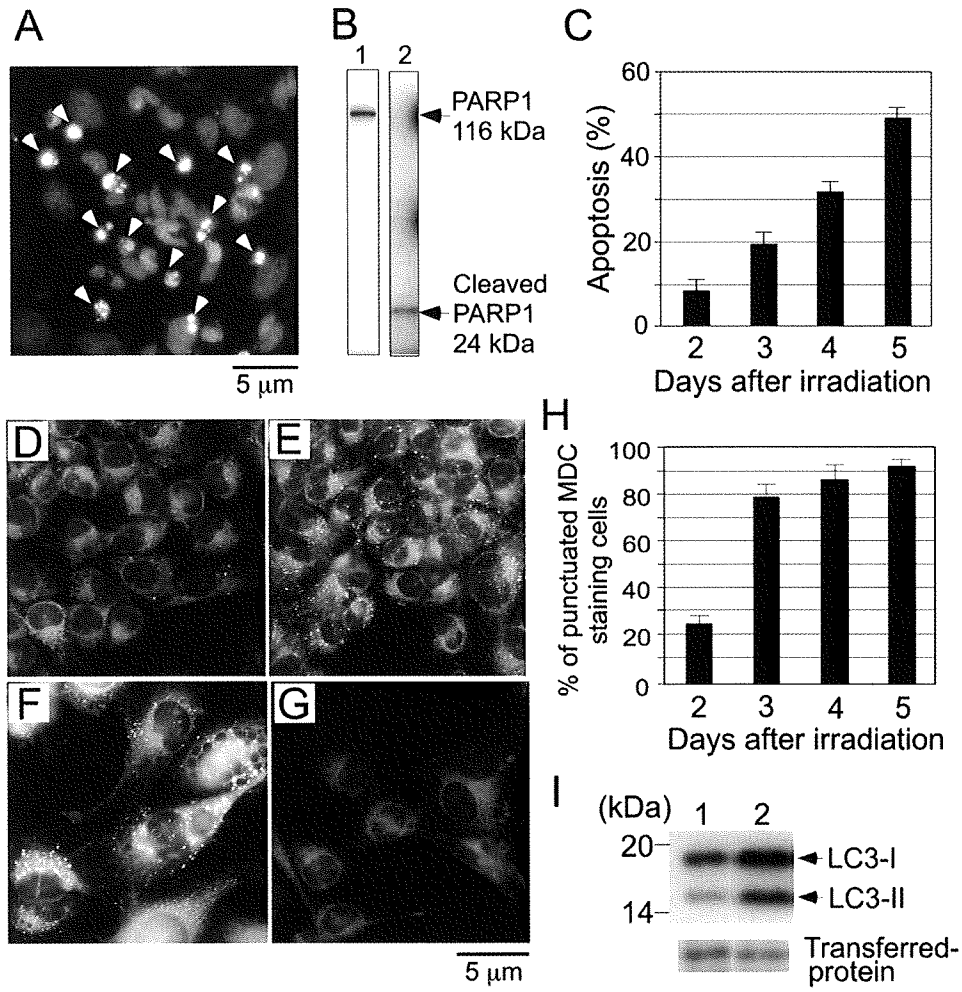

Fig. 2. Induction of apoptosis and autophagy in C-ion–irradiated NP-2 cells. (A) Irradiated NP-2 cells (5 days after irradiation at 6 Gy) were stained with Hoechst 33342. Cells with increased fluorescence or condensed chromatin (arrowheads) were identified as apoptotic cells. (B) Western blot analysis to detect cleaved PARP-1 fragment. Protein samples (10 μg per lane) were prepared from irradiated NP-2 cells (5 days after irradiation at 6 Gy) that had been attached to dishes (Lane 1) or detached from dishes (Lane 2). (C) Graph shows the percentage of Hoechst 33342-positive apoptotic nuclei in NP-2 cells after irradiation with C-ions at 6 Gy. Apoptotic cells were counted on the days indicated and their ratios were expressed as percentage of total cell counts. Data are shown as the means ± SD. (D) NP-2 cells were incubated in medium (control cells) or (E) in HBSS (starved cells) at 37°C for 2 h. Staining cells with monodansylcadaverine (MDC) indicated formation of many punctuated structures (autophagic vacuoles) in the starved cells. (F) Staining of irradiated NP-2 cells (3 days after irradiation at 6 Gy) with MDC indicated the formation of autophagic vacuoles. (G) These autophagic vacuoles were absent in irradiated NP-2 cells treated for 32 h with 5 mmol/l of 3-methyladenine (3-MA), an autophagy inhibitor. (H) Graph shows percentage of punctuated MDC-positive cells. After irradiation at 6 Gy, punctuated MDC-positive cells were counted on the days indicated, and their ratios were expressed as percentages the total number of cells that had been attached to slides; hence the apoptotic cells were excluded from counting of total cells. Data are shown as the means ± SD. (I) Cell lysates prepared from nonirradiated (Lane 1) or irradiated NP-2 cells (3 days after irradiation at 6 Gy) (Lane 2) were analyzed by Western blotting (20 μg of protein per lane) using an antibody specific for LC3. Blots were stained with Ponceau S to determine whether similar amounts of proteins were transferred in each lane.

cells were quite similar to those of senescent cells reported previously (18), we next examined the expression of SA-β-gal activity, frequently used as a senescent marker, in NP-2 cells 7 days after irradiation (Fig. 3A). We detected SA-β-gal–positive and –negative cells after irradiation at 2 Gy. In contrast, when irradiated at 6 Gy, SA-β-gal activity, localizing at perinuclear regions in the enlarged cells, was clearly detected. Whereas dead cells had detached from dishes, limited numbers of attached cells (<1% of initially irradiated cells) became enlarged and positive for SA-β-gal. The percentage of SA-β-gal-positive cells (number of SA-β-gal–positive cells / number of attached cells × 100) was increased in a time-dependent manner (Fig. 3B).

Most SA-β-gal–positive cells do not synthesize DNA

It is known that permanent growth arrest and failure to enter into S-phase are characteristics of the senescent phenotype detected in all cell types (19,20). We examined whether SA-β-gal–positive cells would be in terminal growth arrest. For this, NP-2 cells were irradiated with C-ions at 3 Gy, cultured

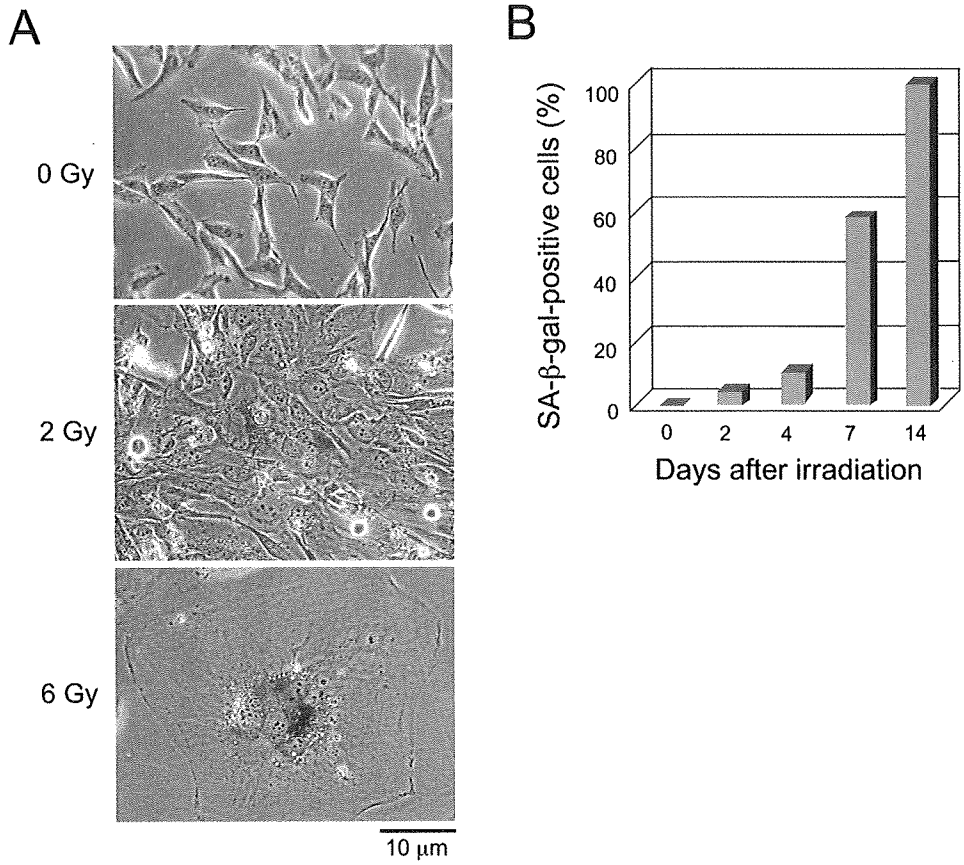

Fig. 3. Detection of Senescence-associated β-galactosidase (SA-β-gal) in NP-2 cells after irradiation with C-ions. (A) SA-β-gal activity was detected in NP-2 cells 7 days after irradiation with C-ions. (B) NP-2 cells were irradiated with C-ions at 6 Gy and cultured. The percentage of SA-β-gal–positive cells was determined as follows: number of SA-β-gal–positive cells/number of attached cells × 100. Experiments were done three times and a representative result is shown.

for 10 days, and labeled with BrdU for 4 h. The cells were then stained for SA-β-gal activity and subjected to anti-BrdU immunohistochemistry. The uptake of BrdU was not detected in nuclei of SA-β-gal–positive large cell, but nuclei of proliferating cells were positive for BrdU signals (Fig. 4A). The ratio of BrdU-positive cells in SA-β-gal–positive cells was determined as 7.7% ± 2.0%, indicating that most SA-β-gal–positive cells did not incorporate BrdU (Fig. 4B).

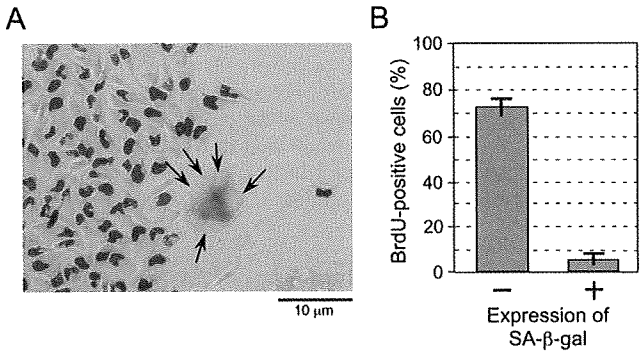

Fig. 4. Double labeling of irradiated NP-2 cells with Senescence-associated β-galactosidase (SA-β-gal) and BrdU. (A) NP-2 cells were irradiated with C-ions at 3 Gy. After 10 days, the cells were labeled with BrdU for 4 h, stained for SA-β-gal, and subjected to anti-BrdU immunohistochemistry. Replicating cells show brown nuclei. Arrows indicate BrdU-negative nuclei of a SA-β-gal-positive multinucleated giant cells (MNGC). (B) Numbers of BrdU-positive cells among in the SA-β-gal–positive or –negative subpopulations.

Detection of another senescence markers in NP-2 cells after C-ion irradiation

Because it has been reported that SA-β-gal activity reflects an increase in lysosomal mass during cellular senescence (21), we stained cells with LysoTracker, a lysosome-specific fluorescent probe (Fig. 5A). Strong perinuclear staining of lysosomes was detected in the irradiated cells at 6 Gy on Day 7, but not in the nonirradiated cells, indicating that C-ion irradiation resulted in an increase in lysosomal mass. In addition, because the accumulation of lipofuscin (a nondegradable intralysosomal polymeric substance) is one of the biomarkers for cellular senescence (22), we examined the expression of lipofuscin by Schmorl reaction (Fig. 5B). Irradiation with C-ions induced specific accumulation of lipofuscin in the enlarged cells, whereas it was absent in the nonirradiated cells. Thus we concluded that although C-ion irradiation induced apoptosis and autophagy in the major population of irradiated cells, cellular senescence was also induced in the residual minor population of irradiated cells.

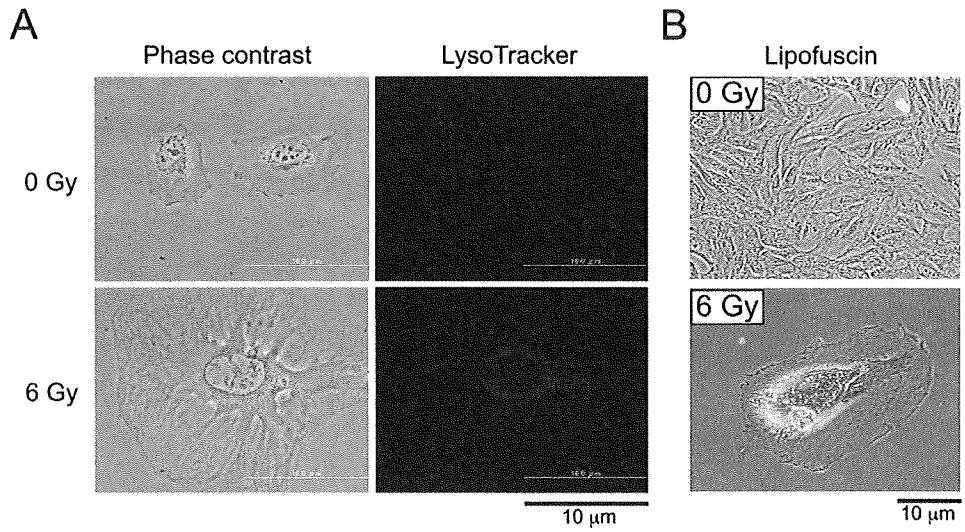

Fig. 5. Detection of senescence-associated increase in cellular lysosomal mass and lipofuscin. (A) LysoTracker was used to stain lysosomes in nonirradiated NP-2 cells or in irradiated cells at 6 Gy and cultured for 7 days. (B) Detection of lipofuscin in NP-2 cells on day 10 after irradiation at 6 Gy.

Effect of C-ion irradiation on the length of telomeres

To examine whether irradiation affects telomere length in NP-2 cells, we determined the mean telomere length (MTL) of NP-2 cells by TRF assay. Southern blot analysis was carried out using $(TTAGGG)_4$ as a probe for digested genomic DNA, and the MTL of nonirradiated cells was determined to be 6.8 kbp long (Fig. 6, lane 7). This MTL was not apparently changed during cultivation for up to 10 days after irradiation at 6 Gy (Fig. 6, lanes 8–10, asterisk). We confirmed that more than 90% of attached cells were positive for the SA-β-gal activity 10 days after irradiation. Therefore, no apparent change of the MTL was detected in the senescent NP-2 cells. However, we also detected DNA fragments longer (~20 kbp) and shorter (~0.6 kbp) than the MTL in samples collected

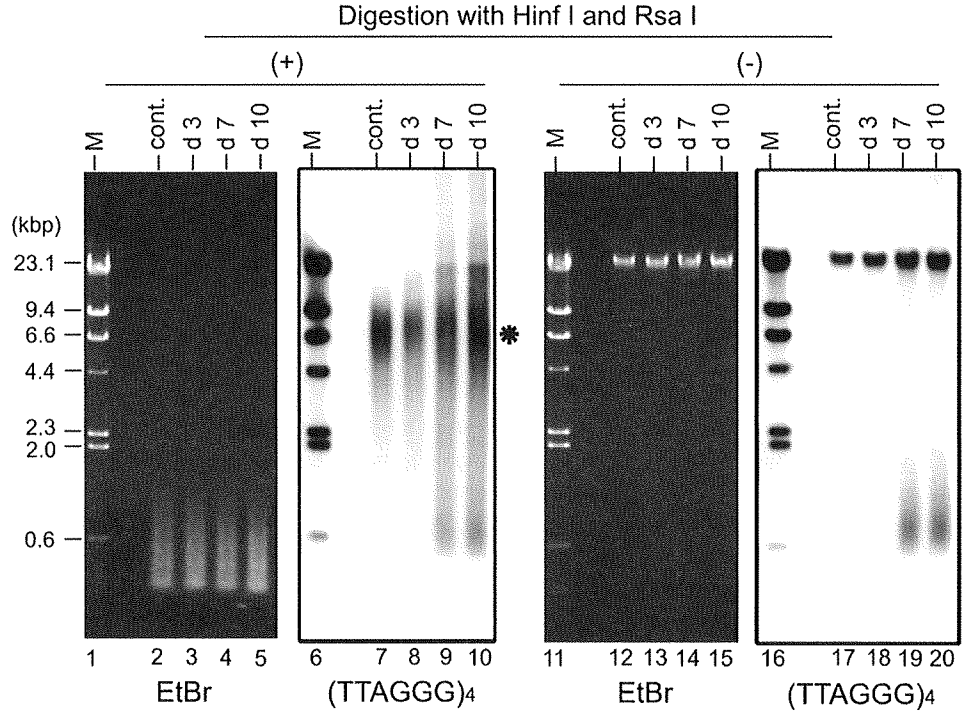

Fig. 6. Telomere length analysis. After various periods of C-ion irradiation at 6 Gy, genomic DNA was prepared, and a telomere restriction fragment (TRF) assay was carried out. Agarose gel was stained with ethidium bromide (EtBr) after electrophoresis, and the blotted filter was hybridized with the digoxigenin (DIG)–labeled telomeric oligonucleotide probe $(TTAGGG)_4$. Each lane was loaded with 0.5 μg of DNA. λ/HindIII DNA (1 μg) per lane was mixed with DIG-labeled λ/HindIII (10 ng) and electrophoresed as a molecular weight marker (M; Lanes 1, 6, 11, and 16). Control DNA was genomic DNA prepared from nonirradiated cells (cont.) (Lanes 2, 7, 12, and 17).

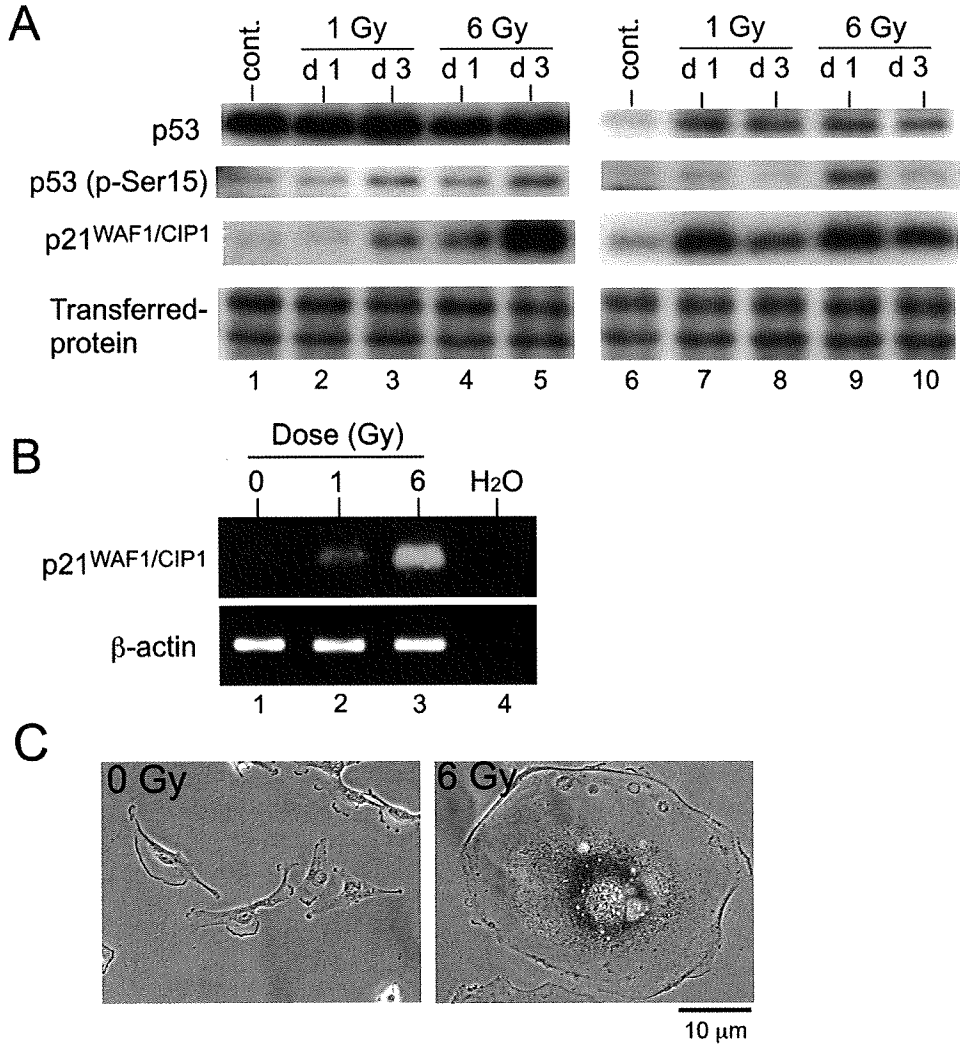

Fig. 7. Detection of p53, phosphorylated p53 (Ser15), and p21$^{WAF1/CIP1}$. (A) NP-2 cells (Lanes 1–5) and U-87MG cells (Lanes 6–10) were irradiated with C-ions, and cell lysates were prepared on the days indicated. Protein samples (20 μg per lane) were analyzed by Western blotting using specific antibodies. Blots were stained with Ponceau S to determine whether similar amounts of total protein were transferred in each lane. Lanes 1 and 6 indicate cell lysates prepared from nonirradiated control cells. (B) Expression of p21$^{WAF1/CIP1}$ mRNA one day after irradiation was detected by reverse transcription–polymerase chain reaction (RT-PCR). β-Actin was used as an internal control. PCR in the absence of cDNA (Lane 4: H_2O) was carried out as a control reaction. (C) Induction of cellular senescence in human glioma cells lacking functional p53. U251-MG cells were irradiated with C-ions (6 Gy), and Senescence-associated β-galactosidase (SA-β-gal) activity was detected 10 days after irradiation.

7 and 10 days after irradiation (Fig. 6, lanes 9 and 10). Smear bands longer than the MTL were not caused by their incomplete digestion with restriction enzymes, because staining with ethidium bromide (EtBr) showed a similar pattern in all samples tested (Fig. 6, Lanes 2–5). As for ~0.6-kbp bands, these fragments were detected even before digestion with the restriction enzymes (Fig. 6, Lanes 19 and 20). Thus our results also suggested that telomere-related chromosomal changes might have occurred in NP-2 cells during the course of induction of cellular senescence.

Detection of p53 and p21$^{WAF1/CIP1}$ in NP-2 cells after C-ion irradiation

We examined expression of tumor suppressor p53 and cyclin/cyclin-dependent kinase inhibitor p21$^{WAF1/CIP1}$ by Western blotting. In addition to NP-2 cells, a human glioblastoma cell line, U-87MG, was examined as a control because the status for p53 in this cell line is reported to be a wild type (23). As expected, expression of p53 in U-87MG cells was increased after irradiation with C-ions (Fig. 7A, Lanes 7–10). Phosphorylation of p53 at Ser15, known to be crucial for p53 stabilization and activation, as well as expression of p21$^{WAF1/CIP1}$ were detected in the irradiated U-87MG cells. On the other hand, high levels of p53 were constitutively expressed in NP-2 cells before and after irradiation (Fig. 7A, Lanes 1–5). To our surprise, as reported by others with different cell types, not only phosphorylation of p53 at Ser15 but also expression of p21$^{WAF1/CIP1}$ was induced in NP-2 cells after irradiation. In addition, RT-PCR showed that the expression of p21$^{WAF1/CIP1}$ mRNA was elevated in

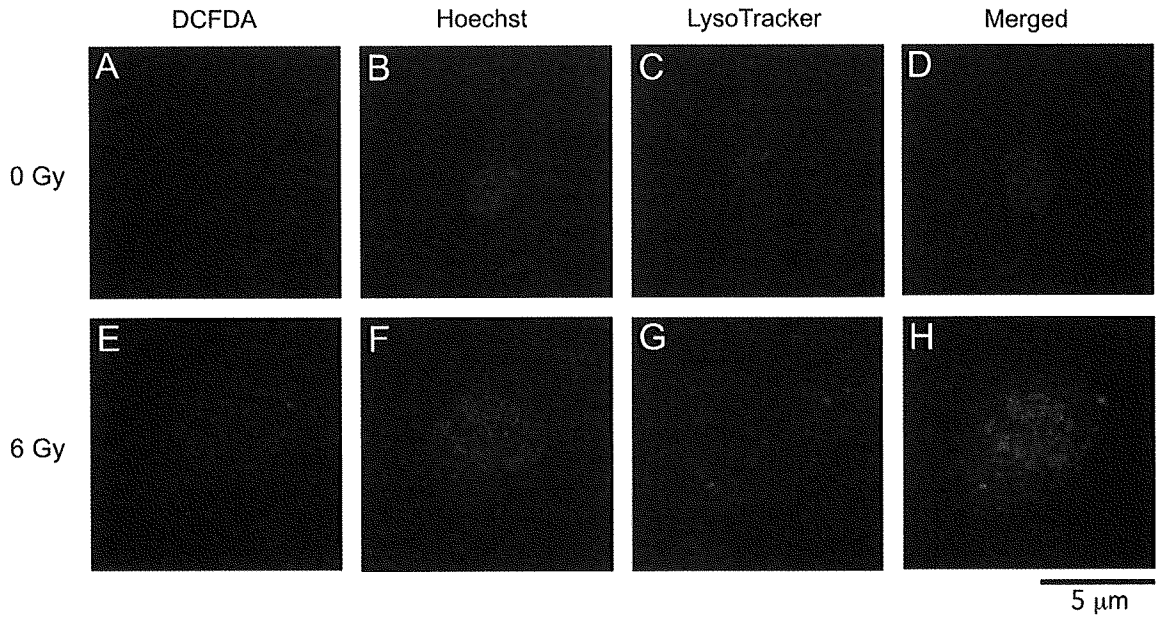

Fig. 8. Enhanced reactive oxygen species (ROS) levels in both nuclear and lysosomal regions of senescent NP-2 cells. Control (A–D) or senescent NP-2 cells (10 days after irradiation with C-ions at 6 Gy) (E–H) were stained with dichlorofluorescein diacetate (DCFDA) (A and E), Hoechst 33342 (B and F), or LysoTracker (C and G), and their images were merged (D and H).

the irradiated cells (Fig. 7B). Thus, these results suggested that the expression of $p21^{WAF1/CIP1}$ plays an important role in the induction of cellular senescence in NP-2 cells after irradiation with C-ions.

We next examined whether irradiation with C-ions would induce cellular senescence in human glioma cells lacking functional p53. For this, we irradiated U-251 MG cells, which have been reported to express a mutant type of p53 (23), with C-ions. As shown in Fig. 7C, SA-β-gal activity was clearly detected in enlarged U-251 MG cells 10 days after irradiation, indicating that C-ion exposure can also induce cellular senescence even in glioma cells lacking functional p53.

Enhanced ROS level in both nuclear and lysosomal regions of senescent NP-2 cells

Because it has been reported that senescent cells accumulate ROS (24), for example, superoxide anions, hydrogen peroxide, and hydroxyl radicals, we examined the level of oxidative stress in senescent NP-2 cells. For this, they were stained with DCFDA, a probe for ROS (25). DCFDA enters cells and is deacetylated by cellular esterases to nonfluorecent dichlorofluorescin (DCFH), which is converted by ROS to fluorescent dichlorofluorescein (DCF). As shown in Fig. 8E, ROS were clearly detected in senescent NP-2 cells after irradiation with C-ions at 6 Gy, but not in nonirradiated cells (Fig. 8A). Co-staining with Hoechst 33324 indicated that ROS were localized in the nuclear and perinuclear regions (Figs. 8E and 8F). Because these perinuclear ROS-positive regions looked similar to the lysosomal regions shown in Fig. 5A, the cells were also co-stained with LysoTracker (Fig. 8 G). Perinuclear ROS-positive regions were colocalized with LysoTracker-positive regions (Fig. 8 H), indicating that enhanced intracellular ROS detected in the senescent NP-2 cells were localized mostly in both the nuclear and lysosomal regions.

Effect of ROS on induction of cellular senescence in NP-2 cells

To examine the effect of oxidative stress on induction of cellular senescence, we first measured ROS levels in NP-2 cells a few days after irradiation. Generation of ROS was markedly enhanced in a time-dependent manner (Fig. 9A). In agreement with this, the expression of an antioxidant enzyme, mitochondrial manganese superoxide dismutase (MnSOD or SOD2), but not cytosolic copper/zinc SOD (CuZnSOD or SOD1), was induced (Fig. 9B). The addition of an antioxidant, α-tocopherol (α-Toc), to the irradiated cells effectively lowered the amount of ROS (Fig. 9C). We next investigated the effect of α-Toc on induction of cellular senescence. The addition of α-Toc induced alteration of cell morphology, such as reduction of the cell size or formation of cytoplasmic processes, and SA-β-gal activity was hardly detectable in these morphologically altered cells (Fig. 9D). As a result, supplementation of irradiated cells with α-Toc markedly reduced the number of SA-β-gal-positive cells (Fig. 9E). We confirmed that α-Toc at concentrations used in this study was not cytotoxic to nonirradiated cells. Thus these results suggest that ROS generation after irradiation with C-ions is involved in the induction of cellular senescence in NP-2 cells.

Induction of cellular senescence in NP-2 cells after irradiation with low-LET X-rays

We also examined the effect of low-LET X-ray irradiation on induction of cellular senescence in NP-2 cells. Irradiation

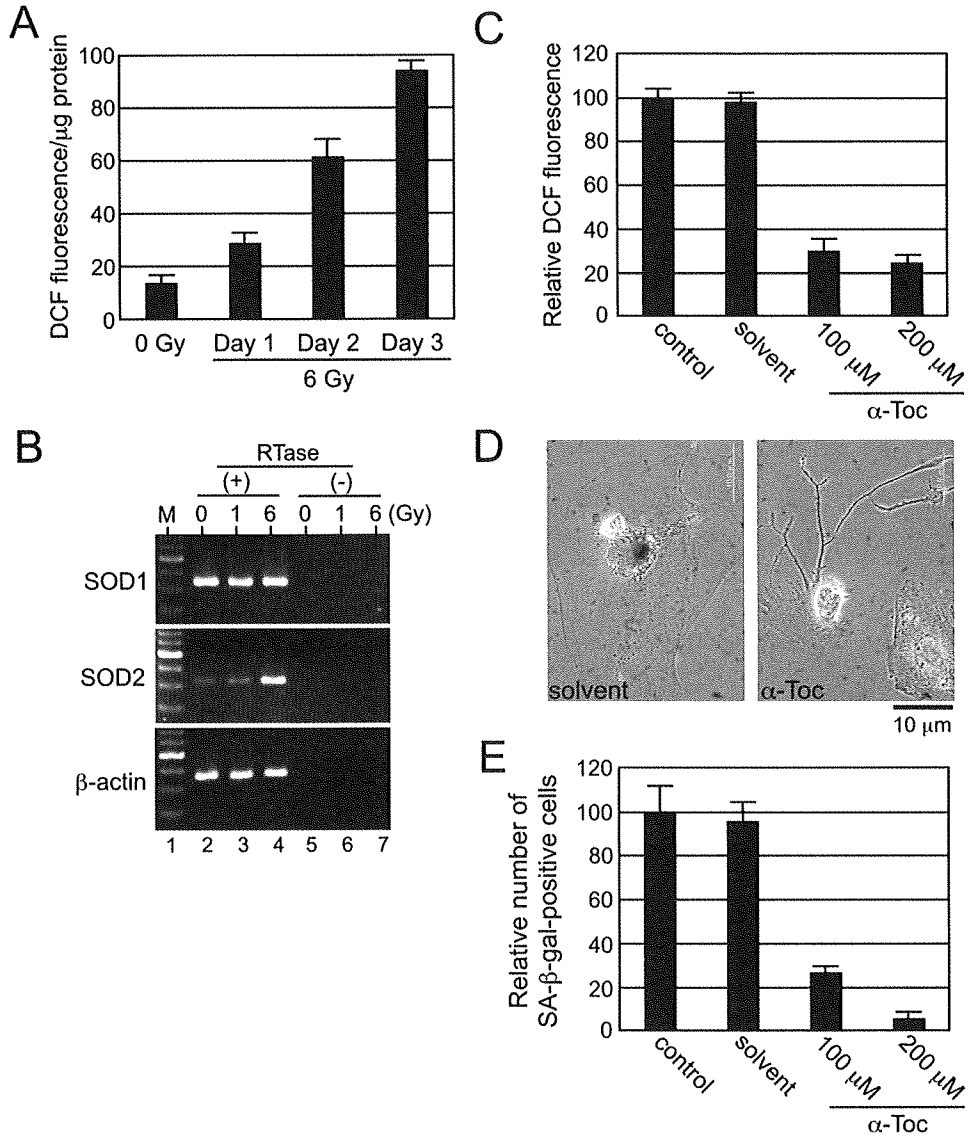

Fig. 9. Effect of reactive oxygen species (ROS) on induction of cellular senescence in NP-2 cells irradiated with C-ions. (A) Determination of ROS levels of NP-2 cells irradiated at 6 Gy by measuring the intensity of dichlorofluorescein (DCF) fluorescence on the days indicated. Means ± standard deviation (SD) of the intensity of DCF fluorescence per cellular protein (μg) are shown. (B) SOD2 but not SOD1 was induced after irradiation. β-Actin was used as an internal control. cDNA was synthesized in the presence (Lanes 2–4) or absence of reverse transcriptase (RTase) (Lanes 5–7). M represents a DNA molecular weight marker (Lane 1). (C) Reduction of ROS in irradiated NP-2 cells after treatment with α-tocopherol (α-Toc). Cells were irradiated at 6 Gy, treated with α-Toc, and DCF fluorescence was measured. α-Toc was dissolved in dimethylsulfoxide as a solvent and diluted in medium. Control cells were treated with medium only. Means ± SD of relative DCF fluorescence are shown. (D) After irradiation of NP-2 cells with C-ions at 6 Gy, the cells were treated with α-Toc (200 μmol/l) and fed with fresh α-Toc every 2 days. Senescence-associated β-galactosidase (SA-β-gal) assay was performed 10 days after irradiation, and cells were photographed. (E) After irradiation of NP-2 cells with C-ions at 6 Gy, they were treated with α-Toc and fed with fresh α-Toc every 2 days. SA-β-gal activity was detected 10 days after irradiation and the relative numbers of SA-β-gal–positive cells are shown as means ± SD.

with X-rays inhibited cell growth in a dose-dependent manner (Fig. 10A), and the D_{10} deduced from the survival curve was 5 Gy (Fig. 10B). The presence of enlarged and flattened cells, one of the senescent markers, was observed in these irradiated cells. In addition, SA-β-gal–positive cells were also detected (Fig. 10C) and their number increased after irradiation in a time-dependent manner (Fig. 10D), indicating that irradiation with low-LET X-rays also induced cellular senescence in NP-2 cells.

DISCUSSION

In this study, we examined biological responses of human glioma cells to irradiation with C-ions. We found that most population of irradiated cells died of apoptosis and autophagy (Fig. 2). Although autophagy is known to be a cytoprotective function associated with nutrient starvation, excess autophagy leads to cell death. Indeed, the time-course experiment indicated that the induction of apoptosis follows autophagy

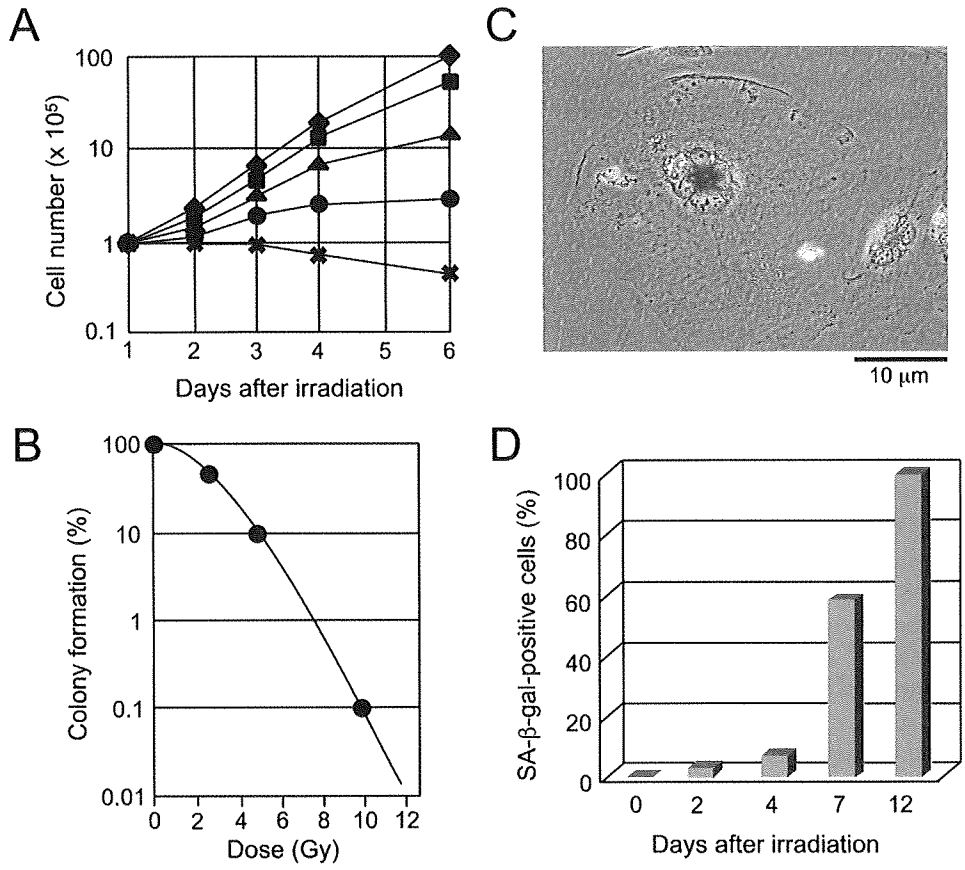

Fig. 10. Induction of cellular senescence in NP-2 cells after irradiation with X-rays. (A) NP-2 cells were irradiated with X-rays at 0 (◆) 2 (■), 5 (▲), 10 (●), or 15 (×) Gy, and the total numbers of cells were counted as shown. (B) After irradiation, a colony formation assay was performed to draw a survival curve. (C) Detection of Senescence-associated β-galactosidase (SA-β-gal) activity in enlarged cells 7 days after irradiation at 15 Gy. (D) NP-2 cells were irradiated with X-rays at 15 Gy and cultured. SA-β-gal–positive cells were counted on the days indicated. Experiments were done three times, and a representative result is shown.

(Figs. 2C and 2 H). Because the functional relationship between autophagy and apoptosis is recognized to be complex (26), further analyses will be required to clarify the role of autophagy in C-ion–induced cell death in NP-2 cells.

Although the induction of apoptosis and autophagy was the major biological response of NP-2 cells to irradiation with C-ions at 6 Gy, we found that only a minor fraction of irradiated cells underwent cellular senescence. Not only C-ions but also X-rays caused cellular senescence in NP-2 cells (Fig. 10). We found that, 7 days after either 6 Gy of C-ions or 15 Gy of low-LET X-rays, premature senescence was induced in NP-2 cells, indicating a dose-dependent LET-effect with relative biological effectiveness (RBE) of approximately 2.5.

The mean telomere length (MTL) of nonirradiated NP-2 cells was determined to be 6.8 kbp long, and no apparent change in the MTL was detected in the senescent NP-2 cells (Fig. 6). Jones *et al.* have previously reported that ionizing radiation induces accelerated senescence but that telomere shortening is not induced (27). In this study, we detected DNA fragments longer (~20 kbp) and shorter (~0.6 kbp) than the MTL in samples collected 7 and 10 days after irradiation, suggesting that telomere-related chromosomal changes might have occurred. It has been reported that telomerase activity participates in the process of DNA repair through synthesis of telomere repeats at DNA double strand breaks (DSBs) (28). Thus the variation in telomere length detected in our study might be caused by telomere-mediated DSB repair, leading to the survival of irradiated cells. More recently, Sgura *et al.* reported a significant increase in telomere length in mammalian cells exposed to low- and high-LET radiations (29). Several *in vivo* and *in vitro* study reports describe the elevation of telomerase activity after exposure to ionizing radiation (30,31), suggesting that there is a relationship between radiosensitivity and telomerase activity (32). Therefore, it will be interesting to examine whether irradiation with C-ions affects the expression and activity of telomerase in NP-2 cells.

Tumor suppressor p53 regulate the induction of growth arrest associated with cellular senescence (27,33–35). We detected p53 in NP-2 cells either before or after irradiation (Fig. 7). However, phosphorylation of p53 at Ser15 as well as expression of $p21^{WAF1/CIP1}$ was detected only after irradiation, suggesting that the induction of $p21^{WAF1/CIP1}$ might be mediated through functional p53 in NP-2 cells. It has been also reported that anticancer agents can induce cellular senescence even in cells lacking functional p53 (36). In this study,

we showed that C-ion exposure also induced cellular senescence in human glioma U-251 MG cells (Fig. 7C), which express a mutant type of p53, indicating that the induction of cellular senescence by irradiation with C-ions is independent of p53.

DNA damage induced by oxidative stress is known to be an important mediator for cellular senescence (8,18,20,37). In this study, we detected elevated ROS levels in NP-2 cells irradiated with C-ions at 6 Gy (Fig. 9A), and ROS elevation was inhibited by addition of α-Toc to irradiated cells (Fig. 9C). Because most of the population of cells died and surviving cells were hardly detectable by colony formation assay when irradiated at 6 Gy (Fig. 1B), even treatment of irradiated cells with α-Toc did not improve cell growth activity and formation of colonies. However, we found that α-Toc inhibited the development of SA-β-gal–positive cells (Figs. 9D and 9E), suggesting that ROS generation contributes to the induction of cellular senescence after irradiation with C-ions.

We also showed that ROS levels were elevated in nuclear and lysosomal regions of the senescent NP-2 cells (Fig. 8). As degradation of iron-containing materials, such as ferritin and mitochondrial metalloproteins, occurs in lysosomal compartments, they are rich in reactive iron (38). This degradation leads to the production of extremely reactive hydroxyl radicals ($HO^{\cdot}$) through interaction between hydrogen peroxide (H_2O_2) and reactive iron in the lysosome. This process is known as the Fenton reaction, and takes place as follows: $Fe^{2+} + H_2O_2 \cdot Fe^{3+} + HO^{\cdot} + OH^{-}$ (38). Although H_2O_2 is mainly produced by mitochondria from superoxide radicals ($^{\cdot}O_2^{-}$) by SOD, it diffuses freely across lysosomal membranes. Actually, we showed that the expression of mitochondrial SOD2 responsible for H_2O_2 production was induced in NP-2 cells irradiated with C-ions (Fig. 9B). Thus, localization of ROS in the lysosomal region of senescent NP-2 cells may be explained that highly reactive $HO^{\cdot}$ was formed in the iron-rich lysosomes through the Fenton reaction.

Glioma/glioblastoma is known as one of the most radioresistant tumors. However, results of C-ion radiotherapy combined with X-ray radiotherapy and chemotherapy in a Phase I/II clinical trial for patients with malignant gliomas at the National Institute of Radiological Sciences in Japan showed potential efficacy of C-ion radiotherapy (39, 40). Thus, additional basic research to elucidate biological responses of glioma cells to C-ions irradiation *in vitro* will contribute to further improvement of C-ions radiotherapy.

CONCLUSION

In summary, we found that a major population of human glioma cells died of apoptosis and autophagy after irradiation with C-ions. C-ion exposure also induced cellular senescence in a minor population of the irradiated cells. Elucidation of a gene(s) and regulatory mechanism(s) of cell death and cellular senescence in response to C-ion irradiation should contribute to developing new therapeutic protocols to improve the efficacy of cancer radiation therapy using heavy ion beams and to reduce its side effects.

REFERENCES

1. Kramer M, Weyrather WK, Scholz M. The increased biological effectiveness of heavy charged particles: From radiobiology to treatment planning. *Technol Cancer Res Treat* 2003;2: 427–436.
2. Tsujii H, Mizoe J, Kamada T, *et al.* Overview of clinical experiences on carbon ion radiotherapy at NIRS. *Radiother Oncol* 2004;73:S41–S49.
3. Hamada N. Recent insights into the biological action of heavy-ion radiation. *J Radiat Res* 2009;50:1–9.
4. Iwadate Y, Mizoe J-E, Osaka Y, *et al.* High linear energy transfer carbon radiation effectively kills cultured glioma cells with either mutant or wild-type p53. *Int J Radiat Oncol Biol Phys* 2001;50:803–808.
5. Tsuboi K, Moritake T, Tsuchida Y, *et al.* Cell cycle checkpoint and apoptosis induction in glioblastoma cells and fibroblasts irradiated with carbon beam. *J Radiat Res* 2007;48: 317–325.
6. Wada S, Kobayashi Y, Funayama T, *et al.* Detection of DNA damage in individual cells induced by heavy-ion irradiation with a non-denaturing comet assay. *J Radiat Res* 2002;43: S153–S156.
7. Ito H, Daido S, Kanzawa T, *et al.* Radiation-induced autophagy is associated with LC3 and its inhibition sensitizes malignant glioma cells. *Int J Oncol* 2005;26:1401–1410.
8. Suzuki M, Boothman DA. Stress-induced premature senescence (SIPS)—influence of SIPS on radiotherapy. *J Radiat Res* 2008; 49:105–112.
9. Hamada N, Funayama T, Wada S, *et al.* LET-dependent survival of irradiated normal human fibroblasts and their descendents. *Radiat Res* 2006;166:24–30.
10. Biederbick A, Kern HF, Elasser HP. Monodansylcadaverine (MDC) is a specific *in vivo* marker for autophagic vacuoles. *Eur J Cell Biol* 1995;66:3–14.
11. Munafo DB, Colombo MI. A novel assay to study autophagy: Regulation of autophagosome vacuole size by amino acid deprivation. *J Cell Sci* 2001;114:3619–3629.
12. Seglen PO, Gordon PB. 3-Methyladenine: Specific inhibitor of autophagic/lysosomal protein degradation in isolated rat hepatocytes. *Proc Natl Acad Sci U S A* 1982;79:1889–1892.
13. Kabeya Y, Mizushima N, Ueno T, *et al.* LC3, a mammalian homologue of yeast Apg8p, is localized in autophagosome membranes after processing. *EMBO J* 2000;19:5720–5728.
14. Dimri GP, Lee X, Basile G, *et al.* A biomarker that identifies senescent human cells in culture and in aging skin *in vivo*. *Proc Natl Acad Sci U S A* 1995;26:9363–9367.
15. Bancroft JD. An introduction to histochemical techniques. London: Butterworths; 1967. p148–175.
16. Baur JA, Wright WE, Shay JW. Analysis of mammalian telomere position effect. *Methods Mol Biol* 2004;287:121–136.
17. Gozuacilk D, Kimchi A. Autophagy as a cell death and tumor suppressor mechanism. *Oncogene* 2004;23:2891–2896.
18. Ben-Porath I, Weinberg RA. The signals and pathways activating cellular senescence. *Int J Biochem Cell Biol* 2005;37: 961–976.
19. Mathon NF, Lloyd AC. Cell senescence and cancer. *Nat Rev Cancer* 2001;1:203–213.
20. Toussaint O, Medrano EE, von Zglinicki T. Cellular and molecular mechanisms of stress-induced premature senescence (SIPS) of human diploid fibroblasts and melanocytes. *Exp Gerontol* 2000;35:927–945.

21. Kurz DJ, Decary S, Hong Y, *et al.* Senescence-associated β-galactosidase reflects an increase in lysosomal mass during replicative ageing of human endothelial cells. *J Cell Sci* 2000;113: 3613–3622.
22. Brunk UT, Terman A. Lipofuscin: Mechanisms of age-related accumulation and influence on cell function. *Free Radic Biol Med* 2002;33:611–619.
23. Van Meir EG, Kikuchi T, Tada M, *et al.* Analysis of the p53 gene and its expression in human glioblastoma cells. *Cancer Res* 1994;54:649–652.
24. Xin MG, Zhang J, Block ER, *et al.* Senescence–enhanced oxidative stress is associated with deficiency of mitochondrial cytochrome c oxidase in vascular endothelial cells. *Mech Ageing Dev* 2003;124:911–919.
25. Halliwell B, Whiteman M. Measuring reactive species and oxidative damage *in vivo* and in cell culture: How should you do it and what do the results mean? *Br J Pharmacol* 2004;142:231–235.
26. Maiuri MC, Zalckvar E, Kimchi A, *et al.* Self-eating and self-killing: Crosstalk between autophagy and apoptosis. *Nat Rev Mol Cell Biol* 2007;8:741–752.
27. Jones K, Elemore L, Jackson-Cook C, *et al.* p53-Dependent accelerated senescence induced by ionizing radiation in breast tumour cells. *Int J Radiat Biol* 2005;81:445–458.
28. Flint J, Craddock CF, Villegas A, *et al.* Healing of broken human chromosomes by the addition of telomeric repeats. *Am J Hum Genet* 1994;55:505–512.
29. Sgura A, Antoccia A, Berardinelli F, *et al.* Telomere length in mammalian cells exposed to low- and high-LET radiations. *Radiat Prot Dosim* 2006;122:176–179.
30. Hande MP, Lansdorp PM, Natarajan AT. Induction of telomerase activity by in vivo X-irradiation of mouse splenocytes and its possible role in chromosome healing. *Mutat Res* 1998;404:205–214.
31. Hyeon Joo O, Hande MP, Lansdorp PM, *et al.* Induction of telomerase activity and chromosome aberrations in human tumour cell lines following X-irradiation. *Mutat Res* 1998;401: 121–131.
32. Ayouaz A, Raynaud C, Heride C, *et al.* Telomeres: Hallmarks of radiosensitivity. *Biochimie* 2008;90:60–72.
33. Mirzayans R, Scott A, Cameron M, *et al.* Induction of accelerated senescence by gamma radiation in human solid tumor-derived cell lines expressing wild-type TP53. *Radiat Res* 2005;163:53–62.
34. Suzuki K, Mori I, Nakayama Y, *et al.* Radiation-induced senescence-like growth arrest requires TP53 function but not telomere shortening. *Radiat Res* 2001;155:248–253.
35. Sugrue MM, Shin DY, Lee SW, *et al.* Wild-type p53 triggers a rapid senescence program in human tumor cells lacking functional p53. *Proc Natl Acad Sci U S A* 1997;94:9648–9653.
36. Chang BD, Broude EV, Dokmanovic M, *et al.* Role of p53 and $p21^{waf1/cip1}$ in senescence-like terminal proliferation arrest induced in human tumor cells by chemotherapeutic drugs. *Oncogene* 1999;18:4808–4818.
37. von Zglinicki T, Saretzki G, Ladhoff J. Human cell senescence as a DNA damage response. *Mech Ageing Dev* 2005;126: 111–117.
38. Kurz T, Terman A, Brunk UT. The role of oxidative stress and lysosomal iron. *Arch Biochem Biophys* 2007;462:220–230.
39. Mizoe JE, Tsujii H, Hasegawa A, *et al.* Phase I/II clinical trial of carbon ion radiotherapy for malignant gliomas: Combined X-ray radiotherapy, chemotherapy, and carbon ion radiotherapy. *Int J Radiat Oncol Biol Phys* 2007;69:390–396.
40. Tsujii H, Mizoe JE, Kamada T, *et al.* Overview of clinical experiences on carbon ion radiotherapy at NIRS. *Radiother Oncol* 2004;73(Suppl 2):S41–S49.

Journal of Tropical Pediatrics Advance Access published July 3, 2009

Research Letter

Evaluation of a Rapid Immunochromatography Strip Test for Detection of Astrovirus in Stool Specimens

Viral gastroenteritis is one of the most common illnesses in humans worldwide [1]. Recently, astroviruses have emerged as significant etiologic agents and have been implicated in about 2–17.5% of cases gastroenteritis in children [2–5]. When outbreaks of diarrhea occur in communities, rapid virus identification is essential to ensure administration of the appropriate treatment and control. For this reason, a rapid and sensitive diagnostic tool, such as the immunochromatography (IC) test, is required. Most recently, two reports on the evaluation of IC test for norovirus detection have been reported [6, 7]. In this study, we evaluate the newly developed IC test for astrovirus detection (IP-Astro V; ImmunoProbe Co., Ltd., Saitama, Japan) in 44 stool samples of pediatric patients with acute gastroenteritis in Japan during January to March 2007.

RT-PCR was used as the reference test for astrovirus detection [8]. To evaluate the sensitivity and specificity of this IP-Astro V test kit, all of the 44 samples were detected for astrovirus antigen by this kit. The IP-Astro V test kit was performed according to the manufacturer's directions. It took only 15–20 min to obtain the result. A positive result consisted of two lines; the left control line (C) and the right (T) positive line. A negative result consisted of a single left control line (C) (Fig. 1).

By the RT-PCR reference method, 10 samples were confirmed as astroviruses. Then, all of the astrovirus-positive samples were further characterized for their genotypes and subtypes by sequencing. It was found that all of the astroviruses found in this study belonged to genotype 1 and clustered closely together in monophyletic branch of 1d subtype (data not shown).

To evaluate sensitivity and specificity of the IP-Astro V kit, a panel of 44 stool samples was tested and the results were compared with those of the RT-PCR method (Table 1). Of the total of 10 samples that were positive for astroviruses by RT-PCR, all were also recognized by this IP-Astro V kit. This result indicated 100% sensitivity. However, three false positives for astrovirus detection were observed, while other 31 samples that tested negative for astrovirus by RT-PCR were also negative by this IP-Astro V kit. These data resulted in a specificity of 91.2%.

The importance of astroviruses as human pathogens has been recognized increasingly due to the improvement of the molecular detection methods [8]. The clinical presentation of patients with symptoms of acute gastroenteritis is generally not indicative of a specific pathogen. Therefore, a rapid and sensitive diagnosis tool for virus detection could be helpful in therapeutic decision making. For this reason, a new IP-Astro V kit was developed. This rapid diagnostic test is easy to perform at the bedside, as it takes only 15–20 min to reach a diagnosis with a simple procedure, and does not require special equipments.

In conclusion, this study demonstrated that the IP-Astro V kit proved to be a rapid method for detection of astroviruses directly from stool samples and may be useful for screening astroviruses during outbreaks of food-borne and person-to-person transmission.

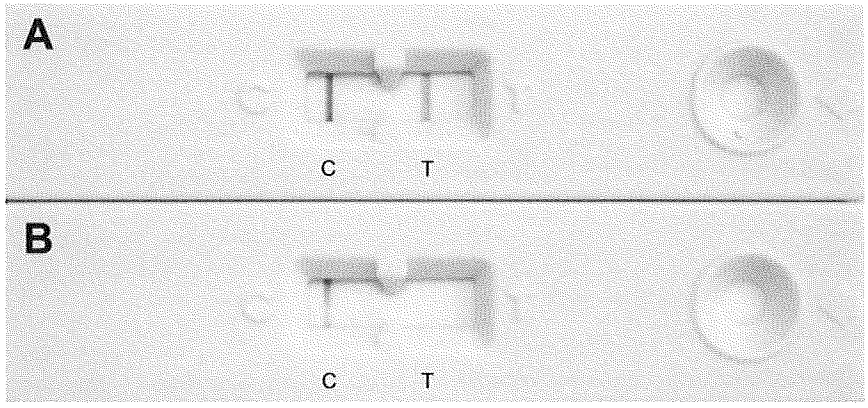

FIG. 1. Detection of NoV in a stool sample by the IP-Astro V kit. The test is positive if two lines appear in the membrane (**A**). The test is negative when only one line appears in the control area (**B**).

doi:10.1093/tropej/fmp055

TABLE 1
Comparison of astrovirus detection in stool samples by IP-Astro V kit and RT-PCR method

	RT-PCR		
	Positive	Negative	Total (%)
IP-Astro V			
Positive	10	3	13 (29.5)
Negative	0	31	31 (70.5)
Total (%)	10 (22.7)	34 (77.3)	44 (100)

PATTARA KHAMRIN,[a] SHUVRA KANTI DEY,[b] WISOOT CHAN-IT,[b] AKSARA THONGPRACHUM,[b] KENJI SATOU,[c] SHOKO OKITSU,[d] NIWAT MANEEKARN,[e] and HIROSHI USHIJIMA[a,b]

[a]*Aino Health Science Center, Aino University, Tokyo, Japan,* [b]*Department of Developmental Medical Sciences, Institute of International Health, Graduate School of Medicine, the University of Tokyo, Tokyo, Japan,* [c]*ImmunoProbe Co. Ltd., Kamagata, Ranzan-machi, Saitama, Japan,* [d]*Aino Health Science Center, Aino college, Tokyo, Japan,* [e]*Department of Microbiology, Faculty of Medicine, Chiang Mai University, Chiang Mai, Thailand*

References

1. Clark B, McKendrick M. A review of viral gastroenteritis. Curr Opin Infect Dis 2004;17:461–9.
2. Dey SK, Islam A, Mizuguchi M, *et al.* Epidemiological and molecular analysis of astrovirus gastroenteritis in Dhaka City, Bangladesh. J Trop Pediatr 2008;54:423–5.
3. Malasao R, Maneekarn N, Khamrin P, *et al.* Genetic diversity of norovirus, sapovirus, and astrovirus isolated from children hospitalized with acute gastroenteritis in Chiang Mai, Thailand. J Med Virol 2008; 80:1749–55.
4. Nguyen TA, Hoang L, Pham le D, *et al.* Identification of human astrovirus infections among children with acute gastroenteritis in the Southern Part of Vietnam during 2005-2006. J Med Virol 2008;80:298–305.
5. Phan TG, Okame M, Nguyen TA, *et al.* Human astrovirus, norovirus (GI, GII), and sapovirus infections in Pakistani children with diarrhea. J Med Virol 2004;73:256–61.
6. Khamrin P, Nguyen TA, Phan TG, *et al.* Evaluation of immunochromatography and commercial enzyme-linked immunosorbent assay for rapid detection of norovirus antigen in stool samples. J Virol Methods 2008;147:360–3.
7. Nguyen TA, Khamrin P, Takanashi S, *et al.* Evaluation of immunochromatography tests for detection of rotavirus and norovirus among Vietnamese children with acute gastroenteritis and the emergence of a novel norovirus GII.4 variant. J Trop Pediatr 2007;53:264–9.
8. Sakamoto T, Negishi H, Wang QH, *et al.* Molecular epidemiology of astroviruses in Japan from 1995 to 1998 by reverse transcription-polymerase chain reaction with serotype-specific primers (1 to 8). J Med Virol 2000;61:326–31.

Acknowledgements

This research was supported by Grants-in-Aid from the Ministry of Education, Culture, Sport, Sciences and Technology and the Ministry of Health, Labor and Welfare, Japan. In addition, this research was supported in part by a Grant-in-Aid for Scientific Research under the JSPS Postdoctoral Fellowships (FY2008). We thank the ImmunoProbe Co., Ltd. (Saitama, Japan) for kindly providing the IP-Astro V kit.

Correspondence: Hiroshi Ushijima, MD, PhD, Aino Health Science Center, Aino University, 2-17-3 Shibuya, Shibuya-ku, Tokyo 150-0002, Japan. Tel./Fax: +81-3-3486-8481.
E-mail: <ushijima-hiroshi@jcom.home.ne.jp>

Journal of Tropical Pediatrics Advance Access published September 11, 2009

Research Letter

Molecular and Epidemiological Trend of Sapovirus, and Astrovirus Infection in Japan

Human sapoviruses (SVs), formerly known as Sapporo-like viruses, are single-stranded positive-sense RNA viruses in the family *Caliciviridae*, which have been found to cause outbreaks of gastroenteritis in children's hospitals and mental health care facilities [1, 2]. SVs can be divided into five genogroups (GI to GV), among which, GI, GII, GIV and GV are identified within humans [1]. Human astroviruses (HAstVs) are non-enveloped, single-stranded positive -sense RNA viruses in the family *Astroviridae*, which may be the second most common cause of viral gastroenteritis in young children [3, 4].

A total of 628 fecal specimens were collected from infants and children with acute gastroenteritis in five different places (Maizuru, Tokyo, Sapporo, Saga and Osaka) in Japan during July 2006 to June 2007. The viral genome was extracted applying a QIAGEN® kit (QIAamp Viral RNA kit; QIAGEN®, Hilden, Germany). Using Polymerase chain reaction (PCR) with specific primers resulted in the identification of AstV and SV [5]. The nucleotide sequences of PCR products positive for SV and HAstV were determined with the Big-Dye terminator cycle sequencing kit and an ABI Prism 310 Genetic Analyzer (Applied Biosystems Inc., Foster City, CA, USA). Phylogenetic and molecular evolutionary analyses were conducted using the MEGA version 3.2 software package, AZ, USA [6].

From 628 fecal specimens tested, 3.8% (24 of 628) were positive for SV, while HAstV was detected in 2.4% (15 of 628). In the present study, SV infection was apparently confined within a period of 6 months (November 2006 to April 2007) and HAstV infection apparently lasted 5 months (January 2007 to May 2007). Most of SV- and HAstV-infected patients were in the 1- to 24-month age group. The distribution of gender in positive cases was 55% in males and 45% in females.

All the SV and HAstV amplicons were characterized for serotypes and genetic relationship with the reference strains based on their capsid regions. Their partial nucleotide sequences were compared with each other as well as with reference SV and HAstV strains available in the DDBJ DNA/GenBank database by BLAST.

SVs detected in this study were clustered into only one distinct genogroup I (Fig. 1A). SV genogroup I clustered into two genotypes (GI/1 and GI/2). SV GI/1 was predominant, followed by GI/2 and accounted for 92% (22 of 24) and 8% (2 of 24), respectively. Analysis of nucleotide and amino acid sequences revealed that SVGI/1 was closely related to Lyon30388/98, Plymouth/92 and Manchester/93 strains. HAstV detected in this study belonged to only genotype (HAstV-1d) (Fig. 1B). CLUSTAL X indicated that these SVs and HAstVs were very similar at the amino acid level as well as at the nucleotide level.

The sequences of SVs and HAstVs detected in the study were submitted to GenBank and have been assigned accession numbers FJ823057-FJ823096, respectively.

The results of this study highlight the impact of SVs and HAstVs in diarrheal diseases among children in five different cities in Japan. In conclusion, our findings suggest that SVs and HAstVs are important enteric viruses coexisting in Japanese infants and children. The epidemiology of HAstV serotypes is only beginning to be addressed in Japan.

SHUVRA KANTI DEY,[a] GIA TUNG PHAN,[b] SHUICHI NISHIMURA,[a] MASASHI MIZUGUCHI,[a] SHOKO OKITSU,[a,c] *and* HIROSHI USHIJIMA[a,d]

[a]*Department of Developmental Medical Sciences, Institute of International Health, Graduate School of Medicine, The University of Tokyo, Tokyo, Japan,* [b]*Department of Microbial Pathogenesis, School of Medicine, Yale University, New Haven, CA, USA,* [c]*Aino Health Research Center, Aino College, Japan and* [d]*Aino Health Research Center, Aino University, Tokyo, Japan*

doi:10.1093/tropej/fmp082

Acknowledgements

This study was supported by Grants-in-Aid from the Ministry of Education, Culture, Sports, Sciences and Technology and the Ministry of Health, Labor and Welfare, Japan.

References

1. Dey SK, Phan TG, Nguyen TA, *et al.* Prevalence of sapovirus infection among infants and children with acute gastroenteritis in Dhaka City, Bangladesh during 2004–2005. J Med Virol 2007;79:633–8.
2. Dey SK, Islam A, Mizuguchi M, *et al.* Epidemiological and molecular analysis of astrovirus gastroenteritis in Dhaka City, Bangladesh. J Trop Pediatr 2008;54:423–5.

doi:10.1093/tropej/fmp082

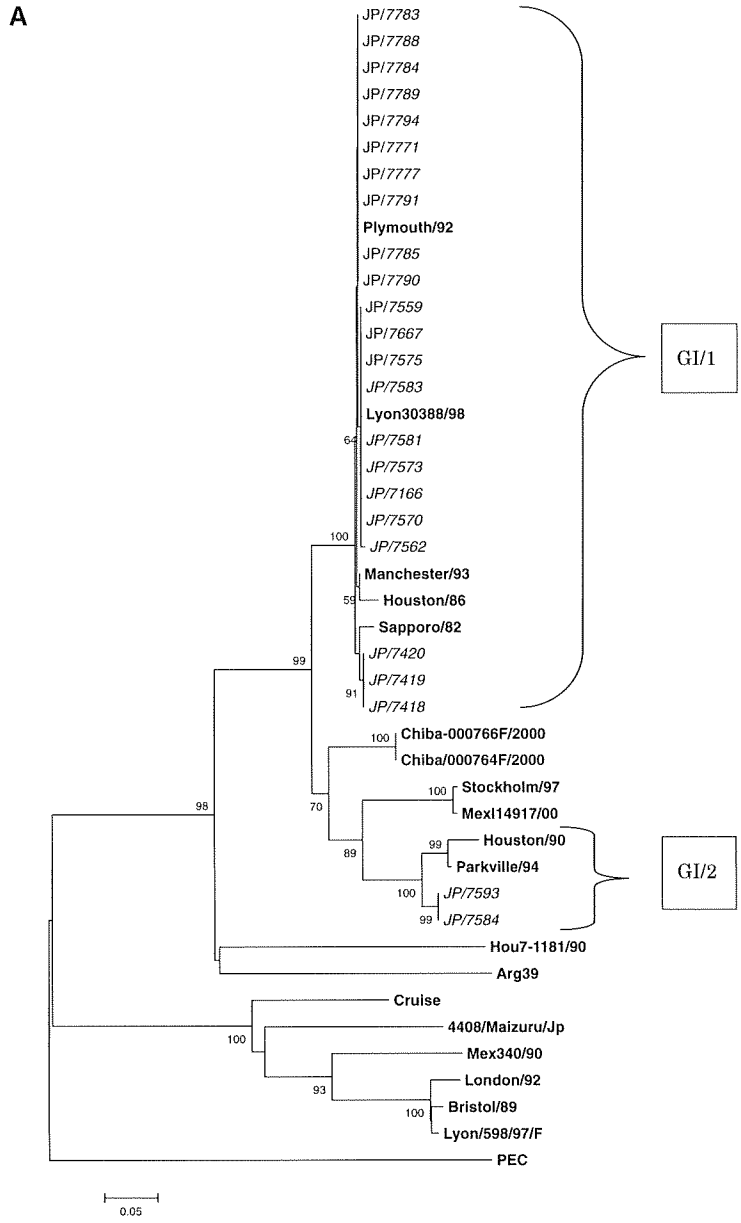

FIG. 1. Phylogenetic tree of nucleotide sequences of Japanese SV and AstV. (**A**) Neighbor-joining phylogenetic tree based on nucleotide sequences of capsid region of SV. (**B**) Neighbor-joining phylogenetic tree based on nucleotide sequences of capsid region of HAstV. The numbers in the branches indicate the bootstrap values. Reference strains of SV and HAstV were selected from DDBJ/GenBank under the accession number indicated in bold. Japanese SVs and HAstVs are highlighted in italics. The scale indicates nucleotide substitutions per position. Reference SV and HAstV strains and their accession numbers used in this study are as follows: SV strains: MexI14917/00 (AF435813), Plymouth/92 (X86559), Lyon30388/98 (AJ251991), Lyon/598/97/F (AJ271056), Chiba-000766F/2000 (AJ412808), Chiba/000764F/2000 (AJ412807), 4408/Maizuru/Jp (AB180209), PEC (AF182760), London/92 (U95645), Mex340/90(AF435812), Cruiseship/00 (AY289804), Hou7-1181/90 (AF435814), Arg39 (AY289803), Stockholm/97 (AF194182), Houston/90 (U95644), Parkville/94 (U73124), Houston/86(U95643), Sapporo/82(U65427), Manchester/93 (X86560) and Bristol98 (AJ249939). HAstV strains: Porcine AstV (AB037272), Dhaka-ast-173 (EU333900), Dhaka-ast-317 (EU333901), AF211956, AY324858, AY720892, EU022556, EU022555, HAstV1 (L23513), HAstV2 (L13745), HAstV6 (L38507) and HAstV4 (L38506).
2 of 3

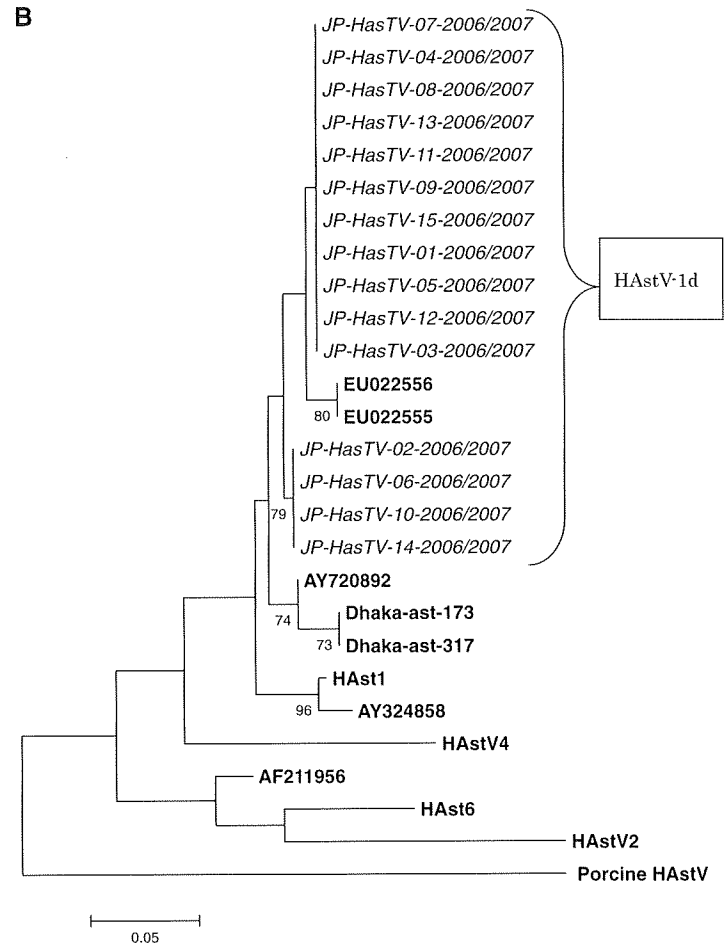

FIG. 1. Continued.

3. Farkas T, Zhong WM, Jing Y, *et al.* Genetic diversity among sapoviruses. Arch Virol 2004;73:1309–23.
4. Guix S, Caballero S, Villena C, *et al.* Molecular epidemiology of astrovirus infection in Barcelona, Spain. J Clin Microbiol 2002;40:133–9.
5. Yan H, Yagyu F, Okitsu S, *et al.* Detection of norovirus (GI, GII), sapovirus and astrovirus in fecal samples using reverse transcription single-round multiplex PCR. J Virol Methods 2003;14:37–44.
6. Kumar S, Tamura K, Jakobsen IB, *et al.* MEGA2: molecular evolutionary genetics analysis software. Bioinformatics 2002;17:1244–5.

Correspondence: Prof. Hiroshi Ushijima, M.D., Ph.D., Department of Developmental Medical Sciences, Graduate School of Medicine, The University of Tokyo,7-3-1 Hongo, Bunkyo-ku, Tokyo 113-0033, Japan. Tel.: (813) 5841-3590; Fax: (813) 5841-3629.

Research Letter

Evaluation of the Newly Developed Immunochromatography Test Kit for Rapid Detection and Differentiation of Norovirus GI and GII

Viral gastroenteritis is one of the most common illnesses in humans worldwide [1]. Noroviruses (NoVs) are considered as the major cause of acute gastroenteritis in both children and adults in community-based gastroenteritis, and responsible for sporadic cases and several outbreaks in various epidemiological settings, including restaurants, schools, day-care centers, hospitals, nursing homes and cruise ships, resulting in over 267 000 000 annual infections worldwide. The common NoV found in humans was GII and GI genogroups [2]. When outbreaks of diarrhea occur in communities, rapid virus identification is essential to ensure administration of the appropriate treatment and control. For this reason, a rapid and sensitive diagnostic tool, such as the immunochromatography (IC) test, is required. Recently, broad reactive monoclonal antibody against several NoV genogroups and genotypes had been produced in our laboratory [3] and several studies on the evaluation of IC test for NoV detections have been reported [4–7].

In this study, the efficacy of the newly developed IC assay (NoV IC; ImmunoProbe Co., Ltd, Saitama, Japan) was evaluated for the rapid detection and differentiation of NoV GI and GII genogroups. By using this kit, NoV could be differentiated as GI or GII genogroup according to the tested line appeared into the strip test. A total of 139 stool specimens collected from children who suffered from acute gastroenteritis in Japan were tested for NoV GI and GII by this NoV IC kit and by a gold standard RT-monoplex PCR method. To evaluate the sensitivity, specificity and agreement for NoV GI and GII genogroups, all of the 139 samples were tested/differentiated as NoV GI and GII by this kit. The NoV IC test kit was performed according to the manufacturer's directions. It took only 15–20 min to obtain the result. A positive result consisted of two or three lines; the left control line (C), the middle positive line for NoV GI (B) and the right positive line for NoV GII (A). A negative result consisted of a single left control line (Fig. 1). To evaluate sensitivity and specificity of the NoV IC kit, a panel of 139 stool

FIG. 1 Detection of NoV in a stool sample by the NoV IC kit. The test is positive for NoV GII if two lines appear in the membrane at A and C positions (**A**), and positive for GI if the lines appear in the membrane at B and C positions (**B**). The test is negative when only one line appears in the control area (**C**).

TABLE 1
Sensitivity, specificity and agreement of NoV detections by NoV IC kit between GI and NoV GII genogroups

NoVIC	Sensitivity *n* (%)	Specificity *n* (%)	Agreement *n* (%)
GI genogroup	71.4	99.2	95.0
GII genogroup	88.8	84.7	87.1

samples was tested and the results were compared with those of the RT-PCR method. These results revealed 71.4 and 88.8% of sensitivity, 99.2 and 84.7% of specificity and 95.0 and 87.1% of agreement for NoV GI and GII detections, respectively (Table 1).

The importance of NoV as human pathogen has been recognized increasingly according to the improvement of the molecular detection methods [8]. The clinical presentation of patients with acute gastroenteritis symptom is generally not indicative of a specific pathogen. Therefore, a rapid and sensitive diagnosis tool for virus detection could be helpful in the therapeutic decision making. For this reason, a new NoV IC kit was developed. This rapid diagnostic test is easy to perform at the bedside, as it takes only 15–20 min to reach a diagnosis with a simple procedure, and does not require special equipments. However, our analysis demonstrated that the sensitivity for NoV GI detection was quite lower than that of GII. Therefore, improvement of the NoV GI detection may need before applying the kit with clinical tests. In conclusion, this study demonstrated that the NoV IC kit was the rapid method for detection and differentiation of NoV GI and GII genogroups directly from stool samples.

PATTARA KHAMRIN,[1] WISOOT CHAN-IT,[2] KENJI SATOU,[3] YUKO NANBA,[3] YASUTAKA YAMASHITA,[4] SHOKO OKITSU,[5] NIWAT MANEEKARN,[6] *and* HIROSHI USHIJIMA[1,2]

[1]*Aino Health Science Center, Aino University, Tokyo, Japan,* [2]*Department of Developmental Medical Sciences, Institute of International Health, Graduate School of Medicine, The University of Tokyo, Tokyo, Japan,* [3]*ImmunoProbe Co. Ltd, Kamagata, Ranzan-machi, Saitama, Japan,* [4]*Ehime Prefecture Institute of Public Health and Environmental Science, Ehime, Japan,* [5]*Aino Health Science Center, Aino college, Tokyo, Japan and* [6]*Department of Microbiology, Faculty of Medicine, Chiang Mai University, Chiang Mai, Thailand*

doi:10.1093/tropej/fmp134

References

1. Clark B, McKendrick M. A review of viral gastroenteritis. Curr Opin Infect Dis 2004;17:461–9.
2. Glass RI, Parashar UD, Estes MK. Norovirus gastroenteritis. N Engl J Med 2009;361:1776–85.
3. Shiota T, Okame M, Takanashi S, *et al.* Characterization of broad reactive monoclonal antibody against norovirus genogroup I and II: recognition of a novel conformational epitope. J Virol 2007;81:12298–306.
4. Khamrin P, Takanashi S, Chan-it W, *et al.* Immunochromatography test for rapid detection of norovirus in fecal specimens. J Virol Methods 2009;157:219–22.
5. Takanashi S, Okame M, Shiota T, *et al.* Development of a rapid immunochromatographic test for noroviruses genogroups I and II. J Virol Methods 2008;148:1–8.
6. Khamrin P, Nguyen TA, Phan TG, *et al.* Evaluation of immunochromatography and commercial enzyme-linked immunosorbent assay for rapid detection of norovirus antigen in stool samples. J Virol Methods 2008;147:360–3.
7. Nguyen TA, Khamrin P, Takanashi S, *et al.* Evaluation of immunochromatography tests for detection of rotavirus and norovirus among Vietnamese children with acute gastroenteritis and the emergence of a novel norovirus GII.4 variant. J Trop Pediatr 2007;53:264–9.
8. Yan H, Yagyu F, Okitsu S, *et al.* Detection of norovirus (GI, GII), Sapovirus and astrovirus in fecal samples using reverse transcription single-round multiplex PCR. J Virol Methods 2003;114:37–44.

Acknowledgements

This research was supported by Grants-in-Aid from the Ministry of Education, Culture, Sport, Sciences and Technology and the Ministry of Health, Labor and Welfare and by a Grant-in-Aid for Scientific Research under the Japan Society for the Promotion of Science Postdoctoral Fellowships (FY2008). We thank (i) the ImmunoProbe Co., Ltd (Saitama, Japan) for kindly providing the NoV IC kit, (ii) Nobuhiro Iritani (Osaka City Institute of Public Health and Environmental Sciences) and (iii) Toshimitsu Tanaka (Chiba City Institute of Health and Environment) for providing some parts of stool samples.

Correspondence: Hiroshi Ushijima, MD, PhD, Aino Health Science Center, Aino University, 2-17-3 Shibuya, Shibuya-ku, Tokyo 150-0002, Japan. Tel./Fax: +81 3 3486 8481. E-mail <ushijima-hiroshi@jcom.home.ne.jp>.

特集 最新版―新生児の感染症

Ⅲ．ウイルスその他の感染

ヒト免疫不全ウイルス（HIV）

山中純子 松下竹次 国立国際医療センター小児科

Key Words
HIV（human immunodeficiency virus：ヒト免疫不全ウイルス）
母子感染
抗ウイルス療法
選択的帝王切開
ZDV（ジドブジン，AZT）

要旨

わが国におけるHIV感染者およびエイズ（AIDS）患者は，近年，増加傾向にある．小児のHIV感染症は頻度が低いとはいえ大部分が母子感染であり，母子感染予防は重要な問題である．ひとたびHIVに感染するとAIDSを発症し，生涯にわたって内服を続けなければならないうえ，集団生活や社会生活の際にさまざまな問題に直面する．HIV母子感染予防策の遂行で母子感染予防が可能になることは，こうした患児を減らすことができるという点で非常に重要なことと思われる．

はじめに

HIV（human immunodeficiency virus）感染症とは，ヒト免疫不全ウイルスがリンパ球（おもにCD4陽性リンパ球）に感染し，徐々に免疫系が破壊されていく進行性の疾患である．最終的には，後天性免疫不全症候群（acquired immunodeficiency syndrome：AIDS）を発症する．

小児HIV感染症の現状としては，USAIDS（国連合同エイズ計画）とWHO（世界保健機関）の2007年の報告によると，世界のHIV感染の推計総数は3,320万人で，このうち1,540万人が女性，250万人が15歳未満の小児であり，AIDSによる死亡者数は210万人（小児42万人）である．世界的にはHIV流行の影響は深刻である[1]．

2007年の厚生労働省エイズ動向委員会によると，わが国におけるHIV感染例は1,082件，AIDS患者も418件と前年より増加を認め，過去最高の報告数となった（図1）．

小児においては，一般的には大部分が母子感染例であるが，2008年度の報告ではわが国の母子感染例は0.5%であり，母子感染予防対策の成果によると考えられる[2]．

本稿では，わが国の現状と母子感染予防の対策について述べる．

HIV母子感染の疫学

2008年度の厚生労働科学研究費補助金エイズ対策研究事業の報告（アンケート調査）によると，1984年からのわが国でのHIV感染女性からの出生児の累計は342例であり，小児HIV感染者およびAIDS患者の累計は45例，非感染例233例，未確定・不明は64例であった（図2）[2]．

予防対策を何も行わなかった場合，母子感染は40%の確率でおこり，児の時期別に発生率が異なる．妊娠中（体内感染）は5～10%，分娩

0386-9806/09/¥100/頁/JCLS

時は10～15%，母乳栄養時期には5～20%が感染することがわかっている[3]．

2008年度の報告では，母児への抗ウイルス療法，予定帝王切開，断乳をすべて実施した群におけるわが国の母子感染率は0.5%であり，HIV母子感染予防対策の成果が認められている[2]．HIV母子感染予防対策マニュアルは厚生労働科学研究費補助金エイズ対策研究事業を中心に改訂を重ねており，予防対策の重要な鍵となっている．

また近年，妊娠早期のHIVスクリーニング検査による感染の診断が積極的に行われるようになり，妊婦のHIV抗体検査率は2008年の報告によると，全国平均で98.3%と年々増加を認めている[2]．

小児HIV感染症で重要なことは，母体のHIVの早期診断により適切な母子感染予防対策（抗ウイルス療法，予定帝王切開，断乳など）をとることで，ほとんどの母子感染を断ち切ることが可能であるという認識をもつことである．

HIV感染予防対策

HIV感染予防対策について，HIV母子感染予防対策マニュアルの第5版（平成19年度）を参

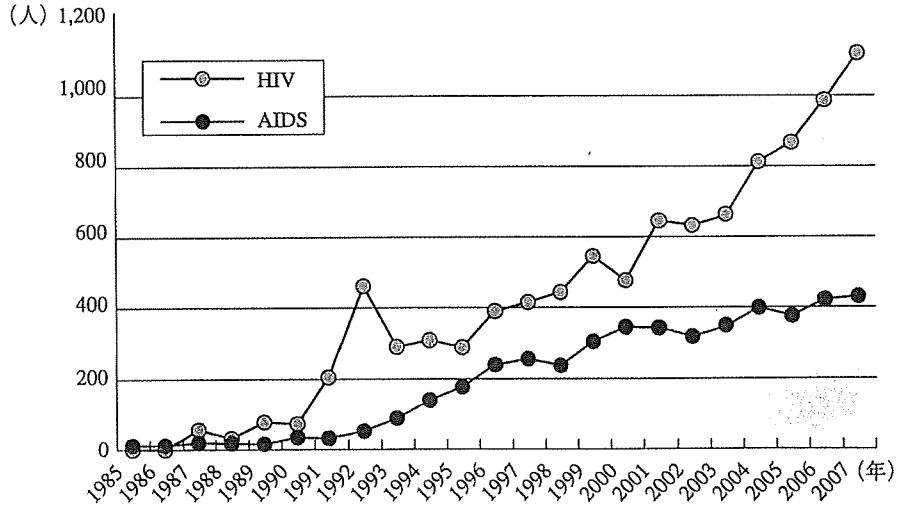

図1 HIV感染者およびAIDS患者報告数の年次推移（文献4）より引用）

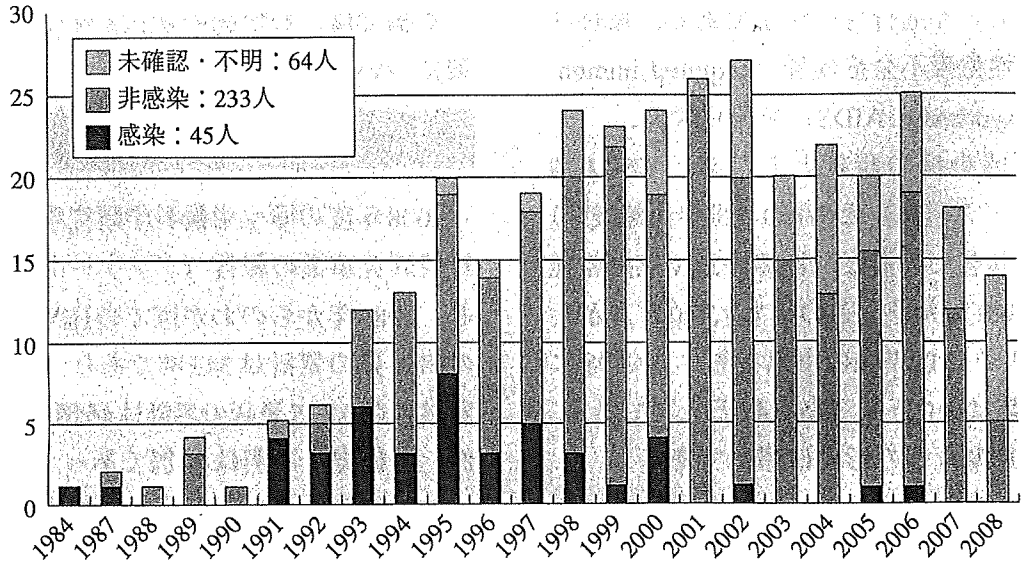

図2 年次別出生数と児の感染状況（2008年度小児科調査，$N=342$）（文献2）より引用）